NANO LETTERS

Letter

pubs.acs.org/NanoLett

Absorbate-Induced Piezochromism in a Porous Molecular Crystal

Christopher H. Hendon,[†] Kate E. Wittering,[‡] Teng-Hao Chen,[§] Watchareeya Kaveevivitchai,[§] Ilya Popov,[§] Keith T. Butler,[†] Chick C. Wilson,[†] Dyanne L. Cruickshank,*[,∥] Ognjen Š. Miljanić,*[,§] and Aron Walsh*[,†]

[†]Department of Chemistry, University of Bath, Claverton Down, Bath BA2 7AY, United Kingdom

[‡]CMAC, EPSRC Centre for Continuous Manufacturing and Crystallization, Department of Chemistry, University of Bath, Bath BA2 7AY, United Kingdom

[§]Department of Chemistry, University of Houston, 112 Fleming Building, Houston, Texas 77204-5003, United States

[∥]Centre for Supramolecular Chemistry Research, Department of Chemistry, University of Cape Town, Rondebosch 7701, South Africa

S *Supporting Information*

ABSTRACT: Atmospherically stable porous frameworks and materials are interesting for heterogeneous solid−gas applications. One motivation is the direct and selective uptake of pollutant/hazardous gases, where the material produces a measurable response in the presence of the analyte. In this report, we present a combined experimental and theoretical rationalization for the piezochromic response of a robust and porous molecular crystal built from an extensively fluorinated trispyrazole. The electronic response of the material is directly determined by analyte uptake, which provokes a subtle lattice contraction and an observable bathochromic shift in the optical absorption onset. Selectivity for fluorinated absorbates is demonstrated, and toluene is also found to crystallize within the pore. Furthermore, we demonstrate the application of electronic structure calculations to predict a physicochemical response, providing the foundations for the design of electronically tunable porous solids with the chemical properties required for development of novel gas-uptake media.

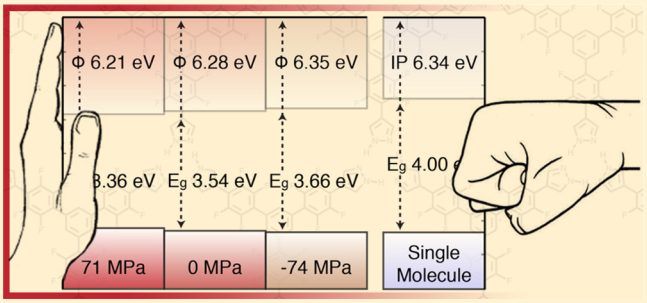

KEYWORDS: *Piezochromism, molecular crystal, density functional theory, bathochromism*

The past 20 years has seen the emergence of designer porous materials, including metal−organic frameworks (MOFs),[1] covalent organic frameworks (COFs),[2] zeolitic imidizolate frameworks (ZIFs),[3] porous molecular cages,[4,5] and less recently, zeolites.[6] Besides uses such as molecular vessels for gas storage and capture,[7−10] success has also been realized through implementation of functional porous materials as light harvesters,[11−13] catalysts,[14,15] and more recently as electroactive species in semiconducting devices.[16−19] There has also been significant progress toward implementation of porous materials in gas sensing and separation applications.[20−23] A limitation is that most hybrid frameworks are chemically unstable in the presence of polar compounds (e.g., water).[24] This instability arises from degradation of the chromophore or macroscopic decomposition stemming from the ionicity of the metal−ligand bond.[25−27]

However, the modularity of hybrid porous materials renders them ideal candidates for heterogeneous applications. To circumvent the softness of the metal−organic bonding, many COFs and zeolitic compounds have been developed, but the exclusion of polar bonds dramatically decreases the material polarization, subsequently resulting in poor gas uptake.[28] In addition, many COFs are based on boronate esters, boroxines, or imines, all of which are hydrolytically labile structural elements.[29,30] It is challenging to design porous frameworks with 3D covalent connectivity and high polarization;[31,32] most COFs have two dimensions of covalent bonding and one dimension of weaker electrostatic adhesive forces (e.g., π-stacking).[33] This connectivity poses problems for gas storage applications, as the electrostatic interactions that cause the sheets to adhere are the same forces that attract and bind guest molecules. More effective gas storage is thus achieved if these forces are orientated into the vacuous pore, rather than between the sheets.

Given the current challenges in increasing guest uptake, porous materials have found success in chemical sensing and separation applications,[34−36] that is, processes that are defined by a physical interaction between the material and absorbate. Because of their inherent softness, these framework materials are particularly good candidates for sensing, as they display large physical responses to small quantities of analyte.[37−40] At low loading levels, in the Henry's law regime, many vacuous materials contract due to the addition of an increased dielectric

Received: January 13, 2015
Revised: February 17, 2015
Published: February 23, 2015

DOI: 10.1021/acs.nanolett.5b00144
Nano Lett. 2015, 15, 2149−2154

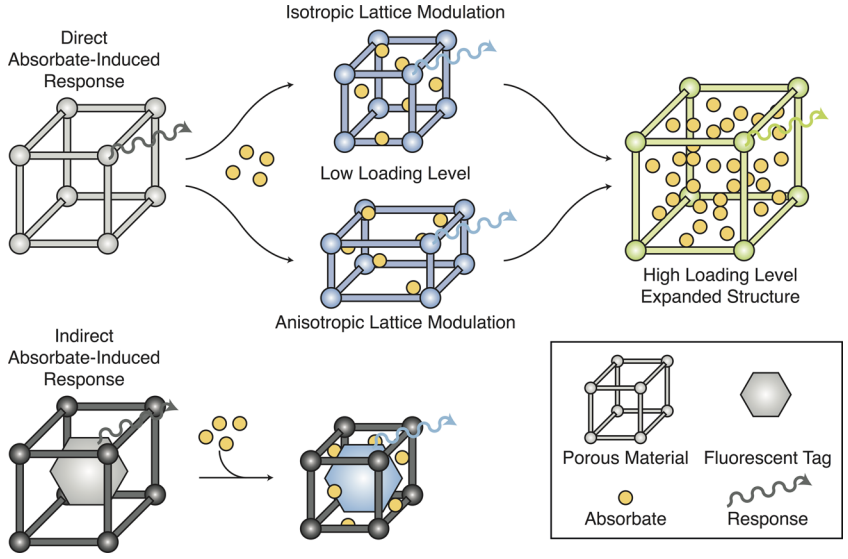

Figure 1. Two approaches for detecting physical modulation of porous materials. In the direct example, the material has a characteristic observable response (gray) upon low-loading of the absorbate (yellow circles) the material is structurally and/or electronically modulated, producing a change in observable response (blue). An indirect measurement relies on a change in material property upon exposure to the absorbate, but the change in observable originates from an indirect (dependent) process, that is, a change in fluorescence of a preloaded fluorophore (hexagon) in the pores.

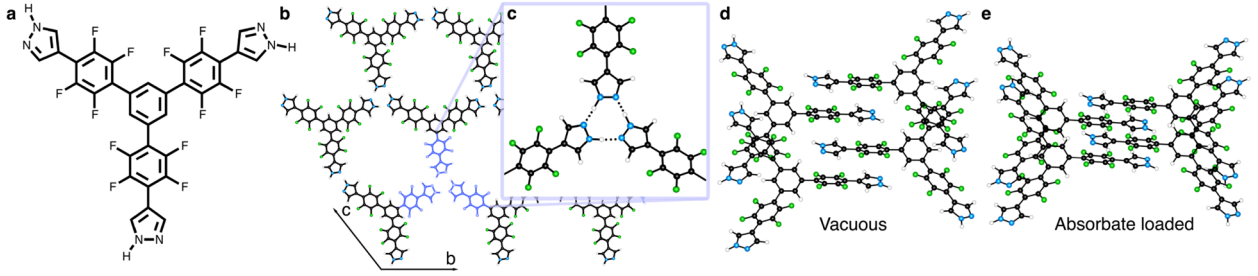

Figure 2. The material examined in this study is a hydrophobic porous molecular crystal, **1**, composed of the fluorinated polyaromatic pyrazole, (a). The material self-assembles into hexagonal channels (b) that are held intraplane through pyrazolic hydrogen bonds (c). The interplane connectivity is similar to the COF series: offset π-stacking. The vacuous structure (d) selectively absorbs fluorinated hydrocarbons, causing a contraction primarily in the $\pi\cdots\pi$ direction (e).

in the pore, which increases the strength of the electrostatic interactions in the framework.[41] This phenomenon can be viewed as a net stabilization of both the guest and framework. Low loading of absorbates can result in either isotropic or anisotropic lattice modulation, as shown in Figure 1. The details of the geometry of the contraction and the elastic response depend on the chemistry of the framework: some bonds are more compressible than others (e.g., $\pi\cdots\pi$ interactions have smaller force constants than covalent bonds).[42−44]

These factors present a challenge in computational prediction and synthetic design of novel porous materials; the variety of chemical compositions and interactions makes physical property predictions difficult. Furthermore, the ideal material must be atmospherically stable and produce an electrical, mechanical, or optoelectronic response upon exposure to absorbates at low concentrations.

Kitagawa and co-workers presented a compelling example of absorbate detection through an indirect response (Figure 1) by preloading a flexible framework with a fluorescent tag.[45] The vacuous capacity is hindered by the inclusion of the fluorescent tag, and the chemical response relies on both the materials and the fluorophore to deform inducing an observable color change. Swager and co-workers suggested a similar approach, where the absorbate quenched a fluorescent marker in the material,[46] however this method relies on the absorbate to be a chromophore. In contrast, Dincă and co-workers recently presented an example of a direct chemical sensing metal−organic framework that produced a change in fluorescence upon metal−ammonia interaction.[47] In both cases, material stability remains a concern.

In this study, we examined the behavior of a fluorinated polyaromatic pyrazolic molecular crystal, **1**, composed of the molecular building block shown in Figure 2a. The solid is a hydrophobic (H_2O contact angle ca. 132°), thermally stable (upper limit ca. 250 °C) porous framework with absorption selectively for fluorinated hydrocarbons.[48] The intraplane connectivity is mediated by hexagonal arrays of pyrazole hydrogen bonds (N−H···N) (Figure 2b,c), while the interplane interaction is defined by the offset π-stacking between electron deficient aromatics and pyrazoles, Figure 2d. Surprisingly for molecular crystals, this solid is chemically stable, as the potentially chemically reactive motifs (the pyrazole hydrogen bonds) are buried within the channel walls. The overall framework is deformable and is more mechanically flexible than the COF series (the rigid boroxine motif is substituted by the hydrogen bound pyrazole system in **1**).

DOI: 10.1021/acs.nanolett.5b00144
Nano Lett. 2015, 15, 2149−2154

The crystal structure of **1** has been redetermined here and was found to crystallize in the monoclinic space group $I2/a$ (a = 7.367 Å, b = 34.52 Å, c = 18.23 Å, β = 91.56°), an alternate setting of the previously reported $C2/c$ structure. Calculations based on density functional theory (DFT) with the HSE06 functional were performed[49] with temperature independent structure parameters within 0.75% of the experimental values (experimental details are included in Supporting Information).

In terms of electronic structure, **1** features a valence band maximum (VBM) and conduction band minimum (CBM) with the same orbital contributions as the single molecule frontier orbitals, drawn in Figure 3. It should be noted that the calculations refer to the occupied and empty electronic band structure and do not probe optical transitions (excited states). Both the molecular and crystal orbitals display characteristic aromatic intramolecular bonding (i.e., π) and antibonding (i.e., π^*) topology. In the perfect solid, the electronic levels of both the VBM and CBM are dependent on intermolecular distance, and the band gap (E_g) is sensitive to the cell pressure. In the equilibrium configuration, solid-state calculations predict E_g = 3.54 eV, which, while not formally equivalent, is in reasonable agreement with the absorption maximum obtained from the spectrofluorescence excitation of the vacuous **1**, λ_{max} = 3.73 eV (332 nm), Table 1.

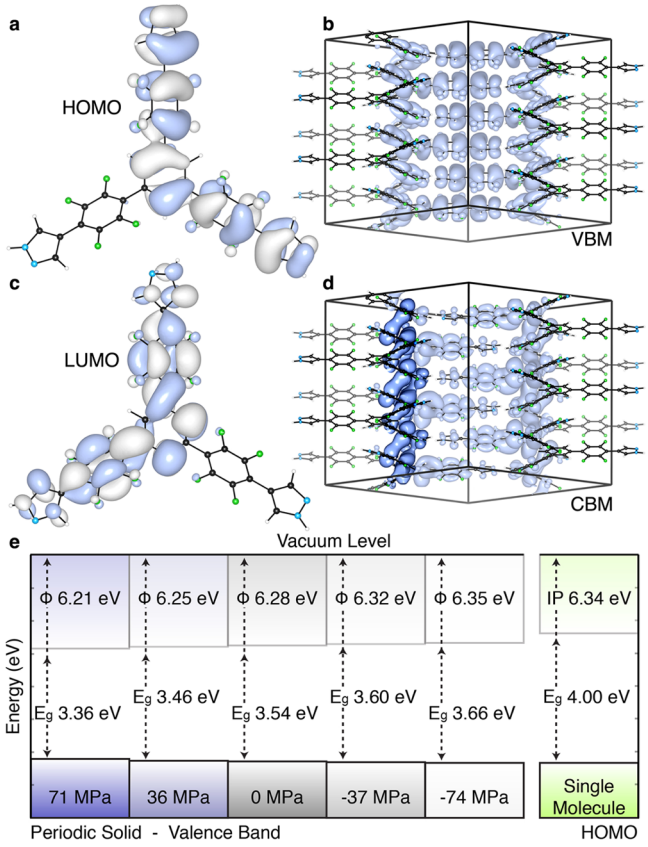

Figure 3. Computed valence band maximum (b) and conduction band minimum (d) of the solid have the same appearance as the molecular building block HOMO (a) and LUMO (c). The electronic structure of **1** is tunable with mechanical pressure: the work function, Φ, and electronic band gap, E_g, of the solid decreases with unit cell contraction (e), independent of absorbate. The five systems represent dilation and contraction by ±2.5% by volume intervals, and their relative external pressures are reported in MPa. The single molecule represents the dilute limit. Isosurfaces from single molecule and periodic HSE06 calculations are drawn to 0.05 and 0.0001 e/Å^3, respectively.

To recover the absolute electron energies (work function) of the porous material, we can align the electronic structure of **1** relative to the vacuum level.[50] The response of the electronic structure to compression and dilation is shown in Figure 3e. The calculated volume deformation potential ($\alpha_V = (dE_g)/(d \ln V)$) is 2.65 eV, that is, a 1% increase in hydrostatic pressure would change the band gap by 0.0265 eV. Material **1** is "soft" with a predicted bulk modulus (B) of 1.21 GPa: the intermolecular π-system is highly compressible and minor changes in the π-stacking direction directly modulate the VBM and CBM energies. The corresponding band gap pressure coefficient ($\alpha_P = -(\alpha_V/B)$) is −2.19 eV/GPa, which is almost 20 times larger than the value for bulk Si.[51] The hydrogen bonding system remains essentially unaltered upon lattice contraction (bond length changes are described in the Supporting Information Table S1).

The origin of the electronic response to stress can be understood by examining the electron density of the frontier bands. Upon compression, the valence band is destabilized as the out-of-phase, destructive, intermolecular π-overlap is increased, resulting in a decreased ionization potential. However, the conduction band intermolecular interactions have a component of constructive wave function overlap, as emphasized in Figure 3d, originating from the spatially helical wave function (the product of the molecular propeller-like geometry) this overlap is stabilized under pressure.[52] It is therefore expected that a decrease in sheet separation should result in a redshift in optical absorption.

In order to verify these predictions, we examined absorbate-specific lattice deformation, optical response and temperature dependence of **1**, both vacuous, and loaded with perfluorohexane, *n*-hexane, benzene, toluene, and cyclohexane. **1** was first "activated" by heating under vacuum at 80 °C for 12 h. The samples were then exposed to each absorbate overnight. From capillary-mode powder X-ray diffraction experiments, it was found that the principal low angle reflections (Figure 4) do not shift with a change in temperature. However, the high-angle reflections (attributed to a-directional reflections) shift to higher 2θ values with a decrease in temperature indicating contraction of the unit cell along the a-axis (the π-stacking direction). Thus, while not formally quantified here, **1** shows anisotropic positive thermal expansion: the hydrogen bound directions appear temperature insensitive, while the π-stacking direction is more susceptible to compression. Flat plate-mode PXRD experiments were conducted to provide additional insights into the contraction of the materials when loaded with various absorbates. All loaded samples displayed similar PXRD patterns to that of the evacuated sample except for the toluene-loaded material (shown in yellow, Figure 4), which contained two additional peaks; this can be attributed to a new evacuation-reversible crystalline material. However, while PXRD confirmed crystallinity, it was found to be insufficient for determining these minor lattice contractions.

Single crystal X-ray diffraction measurements were performed on vacuous **1**, and subsequent absorbate-loaded derivatives. After evacuating **1** under high vacuum for 3 h, single crystal data showed a large void in the material. This vacuous structure remained unchanged after 1 week of exposure to atmospheric conditions (ca. 45% rh, 20 °C). The vacuous structure has a larger cell volume and a-parameter than any of the loaded materials; see Table 1. Upon loading, the

DOI: 10.1021/acs.nanolett.5b00144
Nano Lett. 2015, 15, 2149−2154

Table 1. The 150 K Single Crystal XRD Experimental Lattice Parameters, Spectrofluorescence Absorption Maximum, λ_{max}, and HSE06 Computed Band Gap, E_g, for Each Absorbate[†]

absorbate	*a*	*b*	*c*	*β*	volume (Å^3)	λ_{max} (nm)	E_g (eV)
vacuous	7.3673(7)	34.542(2)	18.225(2)	91.56(1)	4636.1(7)	332	3.73
perfluorohexane	7.29(1)	34.57(6)	18.05(3)	91.1(1)	4549(13)	341	3.64
hexane	7.34(2)	34.5(1)	18.19(6)	91.9(3)	4600(20)	334	3.71
benzene	7.286(6)	34.59(3)	18.30(1)	92.72(6)	4605(6)	333	3.72
toluene	7.34(2)	34.6(1)	18.15(4)	91.7(2)	4611(2)	335	3.70
cyclohexane	‡	‡	‡	‡	‡	334	3.71

[†]There is definitive cell volume and *a*-axis contraction upon uptake of perfluorohexane. Notably, the benzene-loaded material appears to contract in the *a*-axis, however the substantial increase in *β* suggests that the sheetlike structure is slipping out of favorable interaction. [‡]After an exhaustive number of attempts, we could not successfully collect single crystal data on the cyclohexane loaded structure.

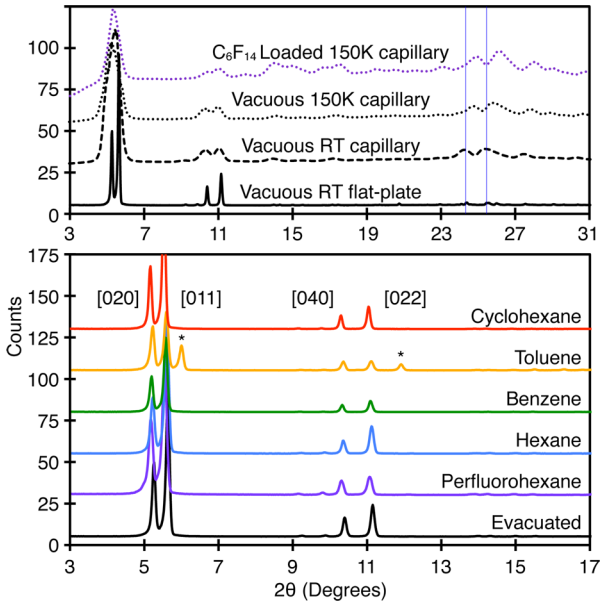

Figure 4. Upper panel: Capillary-mode PXRD shows that low angle reflections, associated with pore dilation, are not significantly altered with temperature or the inclusion of the absorbate. Rather, the high-angle reflections in the *π*-stacking direction are both compressed upon cooling and inclusion of absorbate (emphasized by the blue lines). Higher resolution was achieved with flat-plate PXRD. Lower panel: The flat-plate PXRD was used to confirm the crystallinity of **1** upon loading with the stipulated absorbates. Toluene loading resulted in two new reflections, highlighted by stars.[53]

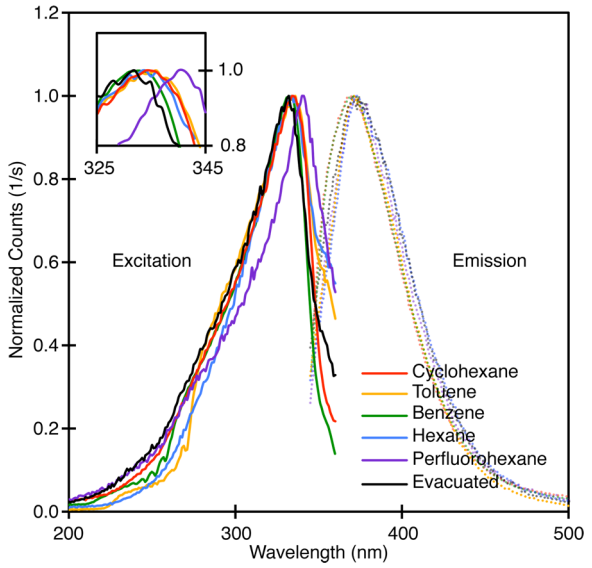

Figure 5. UV−visible spectrofluorescence measurements of vacuous **1** and organic loaded derivatives. Perfluorohexane loaded **1** shows a bathochromic redshift of 9 nm resulting in λ_{max} = 341 nm. Emission λ_{max} = 370−371 nm in all cases.

largest contraction in volume was observed for perfluorohexane, which is not surprising given the reported affinity for halogenated absorbates.[48] The other absorbates all showed very minor volume contraction. Complete single crystal X-ray diffraction data was not obtained for the loaded structures.

The absorbate-induced pressure should cause an optical redshift inversely proportional to cell volume, according to our DFT predictions. To probe this experimentally, UV−vis absorption and fluorescence emission specta were collected using solid-state spectrofluoresence, Figure 5.[54] The absorption λ_{max} redshifts for all absorbates relative to the vacuous structure (corresponding values are listed in Table 1). Importantly, the perfluorohexane loaded **1** (λ_{max} = 341 nm) shows a +9 nm (0.09 eV) red shifted from the vacuous structure (λ_{max} = 332 nm). From our model, this 0.09 eV bathochromic shift corresponds to an effective mechanical pressure of approximately 36 MPa (a low pressure relative to other chemical sensing porous frameworks).[55] All systems show a characteristic emission peak at 370−371 nm. The relaxation process is absorbate-independent; the effective pressure does not alter this peak position.

It is remarkable that such minor lattice deformation is detectable by both X-ray diffraction and optical methods. Furthermore, it is unusual to find porous materials that display a red shift upon contraction. Transitions of this nature are particularly useful in designing sensors that change from colorless to colored upon low level uptake of absorbate.[56−58] Thus, we can envisage further electronic modulation through typical organic functionalization[59] or increased aromatic catenation, pushing this observable response into the visible region.

In summary, the porous molecular crystal examined in this work is a prototype example of where the anisotropy in the chemical bonding (hydrogen bonding and *π*-stacking) is exploited in order to achieve an observable optical response to absorbates, that is, direct chemical detection of fluorinated hydrocarbons. We also note the unusual crystallographic behavior in the presence of toluene. Quantum chemical calculations confirm that the response is driven by electronic modulation within the material with a characteristic band gap pressure coefficient that is an order of magnitude larger than dense materials, dictating the high sensitivity of this material.

DOI: 10.1021/acs.nanolett.5b00144
Nano Lett. 2015, 15, 2149−2154

The design principles found here open up new directions for electronic modulation of porous frameworks.

■ ASSOCIATED CONTENT

Supporting Information

Single crystal data is available in the CCDC, deposit number 1035991. Experimental methods and the electrostatic potential analysis code are also provided. This material is available free of charge via the Internet at http://pubs.acs.org.

■ AUTHOR INFORMATION

Corresponding Authors

*E-mail: (D.L.C.) dyanne.cruickshank@uct.ac.za.
*E-mail: (O.S.M.) miljanic@uh.edu.
*E-mail: (A.W.) a.walsh@bath.ac.uk.

Notes

The authors declare no competing financial interest.

■ ACKNOWLEDGMENTS

The work at the University of Bath benefited by financial support from EPSRC (Grants EP/I033459/1, EP/J017361/1, EP/K004956/1WK, EP/L000202), the Royal Society, the ERC (Grant 277757) and the Leverhulme Trust. The work at the University of Houston is supported by the National Science Foundation (award CHE-1151292), and the Welch Foundation (awards E-0024, E-1571 and E-1768). OŠM is a Cottrell Scholar of the Research Corporation for Science Advancement. Use of the Advanced Photon Source was supported by the U.S. Department of Energy, Office of Science, Office of Basic Energy Sciences, under Contract No. DE-AC02-06CH11357.

■ REFERENCES

(1) Lu, W.; Wei, Z.; Gu, Z.-Y.; Liu, T.-F.; Park, J.; Park, J.; Tian, J.; Zhang, M.; Zhang, Q.; Gentle, T., III; Bosch, M.; Zhou, H.-C. *Chem. Soc. Rev.* **2014**, *43*, 5561−5593.
(2) Feng, X.; Ding, X.; Jiang, D. *Chem. Soc. Rev.* **2012**, *41*, 6010−6022.
(3) Eddaoudi, M.; Sava, D. F.; Eubank, J. F.; Adil, K.; Guillerm, V. *Chem. Soc. Rev.* **2015**, *44*, 228−249.
(4) Dale, E. J.; Vermeulen, N. A.; Thomas, A. A.; Barnes, J. C.; Juríček, M.; Blackburn, A. K.; Strutt, N. L.; Sarjeant, A. A.; Stern, C. L.; Denmark, S. E.; Stoddart, J. F. *J. Am. Chem. Soc.* **2014**, *136*, 10669−10682.
(5) Mitra, T.; Jelfs, K.; Schmidtmann, M.; Ahmed, A.; Chong, S.; Adams, D.; Cooper, A. *Nat. Chem.* **2013**, *5*, 276−281.
(6) Breck, D. W. *Zeolite Molecular Sieves: Structure, Chemistry, and Use*; Krieger: Malabar, FL, 1984.
(7) Herm, Z.; Wiers, B.; Mason, J.; van Baten, J. M.; Hudson, M. R.; Zajdel, P.; Brown, C. M.; Masciocchi, N.; Krishna, R.; Long, J. R. *Science* **2013**, *340*, 960−964.
(8) Zhang, M.; Feng, G.; Song, Z.; Zhou, Y.-P.; Chao, H.-Y.; Yuan, D.; Tan, T. T. Y.; Guo, Z.; Hu, Z.; Tang, B. Z.; Liu, B.; Zhao, D. *J. Am. Chem. Soc.* **2014**, *136*, 7241−7244.
(9) Perry IV, J. J.; Teich-McGoldrick, S. L.; Meek, S. T.; Greathouse, J. A.; Haranczyk, M.; Allendorf, M. D. *J. Phys. Chem. C* **2014**, *118*, 11685−11698.
(10) He, Y.; Zhou, W.; Qian, G.; Chen, B. *Chem. Soc. Rev.* **2014**, *43*, 5657−5678.
(11) Rao, K. P.; Higuchi, M.; Sumida, K.; Furukawa, S.; Duan, J.; Kitagawa, S. *Angew. Chem., Int. Ed.* **2014**, *53*, 8225−8230.
(12) Sippel, P.; Denysenko, D.; Loidl, A.; Lunkenheimer, P.; Sastre, G.; Volkmer, D. *Adv. Funct. Mater.* **2014**, *24*, 3885−3896.
(13) Fracaroli, A.; Furukawa, H.; Suzuki, M.; Dodd, M.; Okajima, S.; Gándara, F.; Reimer, J. A.; Yaghi, O. M. *J. Am. Chem. Soc.* **2014**, *136*, 8863−8866.
(14) Kozachuk, O.; Luz, I.; Llabrés i Xamena, F. X.; Noei, H.; Kauer, M.; Albada, H. B.; Bloch, E. D.; Marler, B.; Wang, Y.; Muhler, M.; Fischer, R. A. *Angew. Chem., Int. Ed.* **2014**, *53*, 7058−7062.
(15) Liu, J.; Chen, L.; Cui, H.; Zhang, J.; Zhang, L.; Su, C.-Y. *Chem. Soc. Rev.* **2014**, *43*, 6011−6061.
(16) Stavila, V.; Talin, A. A.; Allendorf, M. D. *Chem. Soc. Rev.* **2014**, *43*, 5994−6010.
(17) Falcaro, P.; Ricco, R.; Doherty, C. M.; Liang, K.; Hill, A. J.; Styles, M. J. *Chem. Soc. Rev.* **2014**, *43*, 5513−5560.
(18) Talin, A. A.; Centrone, A.; Ford, A. C.; Foster, M. E.; Stavila, V.; Haney, P.; Kinney, R. A.; Szalai, V.; El Gabaly, F.; Yoon, H. P.; Léonard, F.; Allendorf, M. D. *Science* **2014**, *343*, 66−69.
(19) Park, S. S.; Hontz, E. R.; Sun, L.; Hendon, C. H.; Walsh, A.; van Voorhis, T.; Dincă, M. *J. Am. Chem. Soc.* **2015**, *137*, 1774−1777.
(20) For a series of extensive reviews on chemical sensing operational principles and devices refer to *Chem. Rev.* **2008**, *108*, 327−844.
(21) Potyrailo, R. A.; Surman, C.; Nagraj, N.; Burns, A. *Chem. Rev.* **2011**, *111*, 7315−7354.
(22) Schneemann, A.; Bon, V.; Schwedler, I.; Senkovska, I.; Kaskel, S.; Fischer, R. A. *Chem. Soc. Rev.* **2014**, *43*, 6062−6096.
(23) Gao, W.-Y.; Chen, Y.; Niu, Y.; Williams, K.; Cash, L.; Perez, P. J.; Wojtas, L.; Cai, J.; Chen, Y.-S.; Ma, S. *Angew. Chem., Int. Ed.* **2014**, *53*, 2615−2619.
(24) Lee, S.-J.; Bae, Y.-S. *J. Phys. Chem. C* **2014**, *118*, 19833−19841.
(25) Canivet, J.; Fateeva, A.; Guo, Y.; Coasne, B.; Farrusseng, D. *Chem. Soc. Rev.* **2014**, *43*, 5594−5617.
(26) Tiana, D.; Hendon, C.; Walsh, A. *Chem. Commun.* **2014**, *50*, 13990−13993.
(27) Chen, T.-H.; Popov, I.; Kaveevivitchai, W.; Miljanic, O. Š. *Chem. Mater.* **2014**, *26*, 4322−4325.
(28) Murray, L. J.; Dincă, M.; Long, J. R. *Chem. Soc. Rev.* **2009**, *38*, 1294−1314.
(29) Neimark, A. V.; Coudert, F.-X.; Boutin, A.; Fuchs, A. H. *J. Phys. Chem. Lett.* **2010**, *1*, 445−449.
(30) Ortiz, A. U.; Boutin, A.; Fuchs, A. H.; Coudert, F.-X. *Phys. Rev. Lett.* **2012**, *109*, 195502.
(31) Rose, M.; Böhlmann, W.; Sabo, M.; Kaskel, S. *Chem. Commun.* **2008**, *1*, 2462−2464.
(32) Lu, W.; Wei, Z.; Yuan, D.; Tian, J.; Fordham, S.; Zhou, H.-C. *Chem. Mater.* **2014**, *26*, 4589−4597.
(33) Martinez, C. R.; Iverson, B. L. *Chem. Sci.* **2012**, *3*, 2191−2201.
(34) Li, W.; Thirumurugan, A.; Barton, P. T.; Lin, Z.; Henke, S.; Yeung, H. H.-M.; Wharmby, M. T.; Bithell, E. G.; Howard, C. J.; Cheetham, A. K. *J. Am. Chem. Soc.* **2014**, *136*, 7801−7804.
(35) Decoste, J. B.; Peterson, G. W. *Chem. Rev.* **2014**, *114*, 5695−5727.
(36) Davydovskaya, P.; Pohle, R.; Tawil, A.; Fleischer, M. *Sens. Actuators, B* **2013**, *187*, 142−146.
(37) Zhang, G.; Presly, O.; White, F.; Oppel, I. M.; Mastalerz, M. *Angew. Chem., Int. Ed.* **2014**, *53*, 1516−1520.
(38) Zhang, G.; Mastalerz, M. *Chem. Soc. Rev.* **2014**, *43*, 1934−1947.
(39) Nugent, P. S.; Rhodus, V. L.; Pham, T.; Forrest, K. A.; Wojtas, L.; Space, B.; Zaworotko, M. J. *J. Am. Chem. Soc.* **2013**, *135*, 10950−10953.
(40) Chen, L.; et al. *Nat. Mater.* **2014**, *13*, 954−960.
(41) Neimark, A. V.; Coudert, F.-X.; Triguero, C.; Boutin, A.; Fuchs, A. H.; Beurroies, I.; Denoyel, R. *Langmuir* **2011**, *27*, 4734−4741.
(42) Elsaidi, S. K.; Mohamed, M. H.; Wojtas, L.; Cairns, A. J.; Eddaoudi, M.; Zaworotko, M. J. *Chem. Commun.* **2013**, *49*, 8154−8156.
(43) Butler, K. T.; Hendon, C. H.; Walsh, A. *ACS Appl. Mater. Interfaces* **2014**, *6*, 22044−22050.
(44) Woodall, C. H.; et al. *Chem.—Eur. J.* **2014**, *20*, 16933−16942.
(45) Yanai, N.; Kitayama, K.; Hijikata, Y.; Sato, H.; Matsuda, R.; Kubota, Y.; Takata, M.; Mizuno, M.; Uemura, T.; Kitagawa, S. *Nat. Mater.* **2011**, *10*, 787−793.
(46) Yang, J.-S.; Swager, T. M. *J. Am. Chem. Soc.* **1998**, *120*, 11864−11873.

DOI: 10.1021/acs.nanolett.5b00144
Nano Lett. 2015, 15, 2149−2154

(47) Shustova, N. B.; Cozzolino, A. F.; Reineke, S.; Baldo, M.; Dincă, M. *J. Am. Chem. Soc.* **2013**, *135*, 13326−13329.
(48) Chen, T.-H.; Popov, I.; Kaveevivitchai, W.; Chuang, Y.-C.; Chen, Y.-S.; Daugulis, O.; Jacobson, A. J.; Miljanić, O. Š. *Nat. Commun.* **2014**, *5*, 5131.
(49) Krukau, A. V.; Vydrov, O. A.; Izmaylov, A. F.; Scuseria, G. E. *J. Chem. Phys.* **2006**, *125*, 224106.
(50) Butler, K. T.; Hendon, C. H.; Walsh, A. *J. Am. Chem. Soc.* **2014**, *136*, 2703−2706.
(51) Wei, S.; Zunger, A. *Phys. Rev. B* **1999**, *60*, 5404.
(52) Hendon, C. H.; Tiana, D.; Murray, A. T.; Carbery, D. R.; Walsh, A. *Chem. Sci.* **2013**, *4*, 4278−4284.
(53) This new structure was not solved with single crystal methods; however, it is possible that these peaks correspond to discrete ordering of toluene in the pores.
(54) At the time of writing, our solid state UV−visible spectrometer was not functional. Instead, we used a spectrofluorimeter fundamentally probing the UV−vis absorption with the added benefit of a fluorescence measurement.
(55) Cai, W.; Katrusiak, A. *Nat. Commun.* **2014**, *5*, 4337.
(56) Chen, B.; Wang, L.; Zapata, F.; Qian, G.; Lobkovsky, E. B. *J. Am. Chem. Soc.* **2008**, *130*, 6718−6719.
(57) Allendorf, M. D.; Bauer, C. A.; Bhakta, R. K.; Houk, R. J. T. *Chem. Soc. Rev.* **2009**, *38*, 1330−1352.
(58) Hu, Z.; Deibert, B. J.; Li, J. *Chem. Soc. Rev.* **2014**, *43*, 5815−5840.
(59) Hendon, C. H.; Tiana, D.; Fontecave, M.; Sanchez, C.; D'arras, L.; Sassoye, C.; Rozes, L.; Mellot-Draznieks, C.; Walsh, A. *J. Am. Chem. Soc.* **2013**, *135*, 10942−10945.

DOI: 10.1021/acs.nanolett.5b00144
Nano Lett. 2015, 15, 2149−2154